Cell, Vol. 100, 253–263, January 21, 2000, Copyright ©2000 by Cell Press

Maturation Dynamics of a Viral Capsid: Visualization of Transitional Intermediate States

Ramani Lata,* James F. Conway,*# Naiqian Cheng,* Robert L. Duda,† Roger W. Hendrix,† William R. Wikoff,‡ John E. Johnson,‡ Hiro Tsuruta,§ and Alasdair C. Steven*‖
*Laboratory of Structural Biology
National Institute of Arthritis
Musculoskeletal and Skin Diseases
Bethesda, Maryland 20892
†Department of Biological Sciences
University of Pittsburgh
Pittsburgh, Pennsylvania 15260
‡Department of Molecular Biology
The Scripps Research Institute
La Jolla, California 92037
§SSRL/SLAC
Stanford University
Palo Alto, California 94309

Summary

Typical of DNA bacteriophages and herpesviruses, HK97 assembles in two stages: polymerization and maturation. First, capsid protein polymerizes into closed shells; then, these precursors mature into larger, stabler particles. Maturation is initiated by proteolysis, producing a metastable particle primed for expansion—the major structural transition. We induced expansion in vitro by acidic pH and monitored the resulting changes by time-resolved X-ray diffraction and cryo–electron microscopy. The transition, which is not synchronized over the population, proceeds in a series of stochastically triggered subtransitions. Three distinct intermediates were identified, which are comparable to transitional states in protein folding. The intermediates' structures reveal the molecular events occurring during expansion. Integrated into a movie (see Dynamic Visualization below), they show capsid maturation as a dynamic process.

Introduction

Capsid maturation is an essential step in the replication cycles of many viruses and generally involves a major conformational transformation of a precursor particle—the prohead or procapsid (review: King and Chiu, 1997). In some such viruses, this precursor must be processed by a viral protease for maturation to proceed, and inhibition of this enzyme is an attractive target for antiviral drugs, as in the cases of HIV (Wlodawer and Erickson, 1993) and cytomegalovirus (Flynn et al., 1997). For other viruses, maturation is triggered by the onset of DNA packaging. The protein composition of the procapsid may change in maturation: internal scaffolding proteins may be degraded and/or expelled, and additional proteins may bind to the outer surface. Invariably, however, the proteins of the surface shell undergo a cooperative, irreversible, transformation that is remarkable for the magnitude of the accompanying conformational changes.

Bacteriophage HK97 (Hendrix and Duda, 1998) provides an advantageous model system for studying the process of capsid maturation. Its assembly pathway (Figure 1) is distinguished by the following features: (1) a single protein forms both the pentons and the hexons of the $T = 7$ surface lattice and is capable of self-assembly in vivo or in vitro into the earliest precursor, Prohead I; (2) Prohead I is converted to Prohead II by excision of the amino–terminal 11 kDa of the 42 kDa capsid protein; (3) Prohead II is a metastable particle whose transition to the Head I state may be induced in vitro by any of several chemical stimuli (Duda et al., 1995a); (4) in Head I, covalent cross-links form between neighboring subunits, producing Head II, the endstate (Duda, 1998).

On this pathway, the most pronounced structural changes take place in the Prohead II–Head I conversion, which entails major alterations in particle size (expansion by ~25%), shape (near-spherical to polyhedral), and capsomer structure (Conway et al., 1995). The scale of these changes raises the question of how such a radical transformation may be effected while maintaining the physical integrity of the particle. Related questions concern the range of conformational variability that may be exhibited by the subunits of a given particle and the extent to which particles continue to observe icosahedral symmetry during the transition. In general terms, we can envisage at least two possible mechanisms: (1) the transition is divided into a series of steps, each involving a relatively conservative subtransition; (2) a single convulsive transition is initiated locally and propagates in a wave-like manner over the particle (Steven and Carrascosa, 1979). The former mechanism invokes a greater degree of conformational coherence over the transforming particle and anticipates the possibility of multiple short-lived, relatively symmetric, intermediates. The latter mechanism envisages widely differing conformations exhibited by subunits in different parts of the same particle and the eventuality of highly distorted intermediates. However, the two ideas are not mutually exclusive: mechanism (2) may apply to the transitions between intermediates generated by mechanism (1).

We have investigated dynamic aspects of prohead maturation by exploiting the ability of acidic pH to induce conversion of HK97 Prohead II to Head I in a controlled manner (Duda et al., 1995a). Agarose gel electrophoresis experiments indicated that when Prohead II is switched to a pH of ~4, maturation takes place relatively slowly (i.e., over minutes to hours). Under these conditions ("acid-induced" maturation), the course of the reaction was monitored by time-resolved low-angle X-ray diffraction and cryo–electron microscopy (cryo-EM). The former approach afforded continuous sampling of the bulk population, while the latter approach allowed us to determine how many distinct species were present at each

‖To whom correspondence should be addressed (e-mail: alasdair_steven@nih.gov).
#Present address: Institut de Biologie Structurale J.-P. Ebel, F-38027 Grenoble, France.

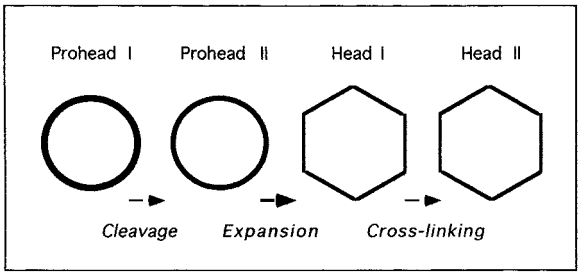

Figure 1. Assembly Pathway of the HK97 Capsid
The major structural changes take place in the expansion step.

time point and in what proportions. Cryo–EM also allowed us to identify and calculate the structures of two transitional intermediates, Expansion Intermediates I and II (E-I and E-II), of acid-induced maturation. Both approaches revealed that the endpoint of this pathway is not, in fact, Head I or Head II, but a particle called Expansion Intermediate III (E-III). E-III is stable at pH 4.18 but, if restored to neutrality, matures to the Head II state (the "acid pulse" pathway).

Results

Our strategy was to establish conditions under which expansion would take place slowly enough that the time course of the reaction could be sampled effectively by both physical techniques employed—X-ray solution scattering and cryo–electron microscopy. Of the various additives that have been shown to induce Prohead II particles to expand (Duda et al., 1995a), acidic pH was chosen for systematic evaluation. Using agarose gel electrophoresis to monitor expansion (Figure 2a), we found that its rate is sensitive to small differences in pH ~4, with half-lives ranging from a few minutes to several hours. For example, a pH of 4.03 resulted in a half-life for expansion of 4–8 min; pH 4.18, in a half-life of about 30 min; whereas at pH 4.36, expansion was extremely slow.

Low-Angle X-Ray Scattering

Solution scattering curves were recorded at 1 min intervals over a period of 30 min, after acidifying a Prohead II preparation at 16 mg/ml to pH 4.0 (Figure 2b). These data registered substantial changes over time, the reaction being at or near completion by 30 min. Inspection of the curves gave no indication of discrete intermediates between the initial and final time points; rather, each curve could be adequately described as a linear combination of the initial and final curves. The transition was about 50% complete at 10 min.

"Static" X-ray solution scattering patterns were recorded for Prohead II and Head. These data were collected for longer and thus were less noisy than in the time-resolved experiment. These curves were distinctly different from each other (Figure 2c). Fitting of spherical shell models indicated inner and outer radii of 220 Å and 248 Å, respectively, for Prohead II, and 273 Å and 294 Å for Head.

The final (t = 30) curve in the time-resolved experiment

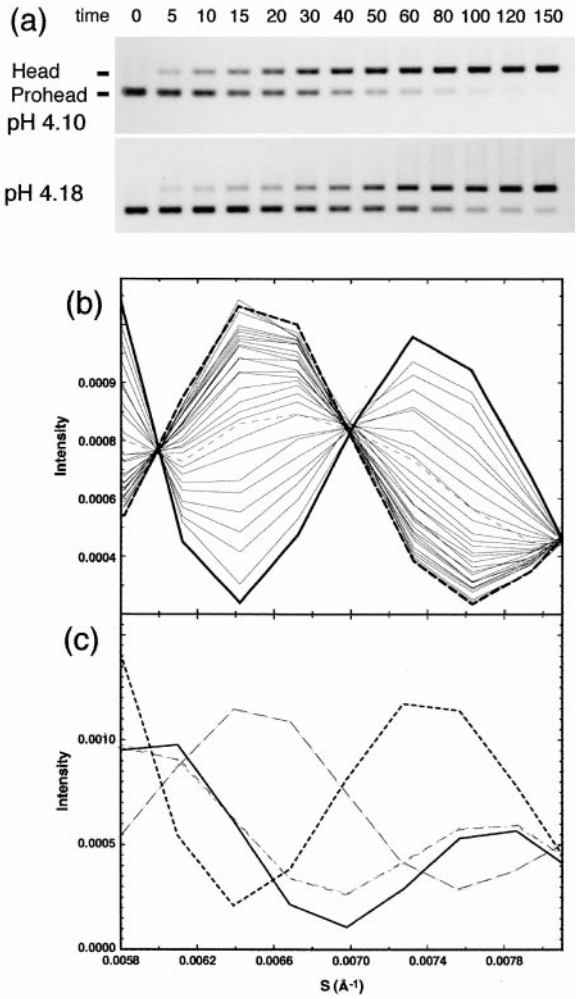

Figure 2. Time Course of Prohead II Expansion at Low pH Monitored by Agarose Gel Electrophoresis and X-ray Solution Scattering

(a) Prior to electrophoresis, samples were diluted 8-fold into 0.2 M KCl, 50 mM Na-acetate at pH 4.10 or 4.18. After the indicated times (min), they were neutralized by diluting 10-fold into 20 mM Tris HCl, 40 mM NaCl, pH 7.5, and run on 1% gels in TAMg buffer (40 mM Tris, 20 mM acetic acid, 1 mM Mg sulfate, pH 8.1). The t = 0 sample was diluted directly into 50 mM Tris-HCl, 0.2 M KCl, pH 7.5. Protein was detected with Coomassie brilliant blue. For the X-ray diffraction experiments, only data between 172–123 Å are shown. Intensity (after background subtraction) is plotted as a function of resolution, *s* (1/Å). (b) Time-resolved spectra recorded at 1 min intervals after acidification. Heavy solid line = data from the t = 1 (min) time point; heavy dashed line = data from the final time point, t = 30. At t = 10 (light dashed line), the reaction was ~50% complete. (c) "Static" solution scattering curves from Prohead II (short bold dashes), Head II (solid line), and Prohead II after 30 min at pH 4.0 (long dashes—inferred to be E-III). After this sample was neutralized to pH 8.3, its spectrum (short light dashes) approximated that of Head II.

was measurably different from that of Head II and yielded an optimal fit with inner and outer radii of 253 Å and 276 Å. This is intermediate in size and shell thickness between Prohead II and Head II, indicating that the endpoint state reached by Prohead II at pH 4.0 differed from both of these particles. When the sample was neutralized, a final scattering curve collected 10 min later (Figure 2c) was indistinguishable from that of Head II.

Time-Resolved Cryo–Electron Microscopy

Although techniques have been developed for studying mixing-initiated reactions on timescales of a few milliseconds by cryo-EM (Berriman and Unwin, 1994; Walker et al., 1995), we considered that conventional grid-quenching offered the best prospects of imaging large fields of particles for many time points in a single experiment. With this approach, the actual freezing takes place in about a millisecond, but grid-handling manipulations limit the frequency of sampling by a single operator to ~5 min per grid. Accordingly, we chose a pH of 4.18 for these experiments (see above).

The Acid-Induced Maturation Pathway

A preparation of Prohead II was shifted from pH 7 to 4.18 and sampled for cryo-EM at progressively increasing intervals over the following 48 hr. In all, 13 grids were prepared, and micrographs adequate for analysis were obtained from all of them. Representative images from the 0 min, 37 min, 152 min, and 8 hr time points are shown in Figure 3. In the control grid made just before the pH switch, i.e., the t = 0 sample, the large majority of particles (>95%) was indeed Prohead II, but a small fraction was visibly larger (by ~8%) and a few distinctively angular, thin-walled, Heads were also present. At subsequent time points, the micrographs showed mixed populations of particles.

From the earliest time sampled (5 min), without clear exception, all particles were already different from Prohead II, being 8%–10% larger. Over the following several hours, the particles were mostly of this size and had the same general appearance, but it was not evident how many subspecies were present. Our strategy for identifying homogeneous subsets involved a two-step classification: first, according to size; then, according to structure. Size discrimination was performed by comparing each particle in turn with reprojections of variously scaled copies of a common model, and assigning it to the size class that gave the highest correlation coefficient (see Experimental Procedures). Working iteratively in this way, we aimed to home in on a self-consistent set of distinct particles. From this analysis, we currently distinguish only two particles of this size with confidence: E-I, which predominated at t = 5 min, and E-II, which predominated at t = 120 min. However, we suspect that the number of subtly different intermediates in this size range may be larger.

Beyond 2.5 hr, we began to observe increasing numbers of a particle with unmistakable attributes that we call E-III. It is thin walled and round, and shows very little variability in appearance from particle to particle. These properties imply either that these particles (unlike the others) preferentially adopt orientations in which they are viewed along a 5-fold symmetry axis or that they are near-spherical in shape. Further analysis (below) confirmed the latter alternative.

The main conclusions to emerge from these observations may be summarized as follows: upon acidification to pH 4.18, Prohead II rapidly switches into a partially expanded state, E-I. Over the next few hours, it remains at much the same size, but remodeling of its capsomers continues to take place. We currently recognize one additional intermediate of this size, E-II. The next development is the balloon-like particle, E-III, which is round and thin walled. First observed in significant numbers at ~4 hr, E-III forms the majority population by t ≈ 8 hr, and if the pH is maintained at pH 4.18, the capsids remain indefinitely in this state. However, if the pH is restored to neutrality, they convert to mature polyhedral Heads.

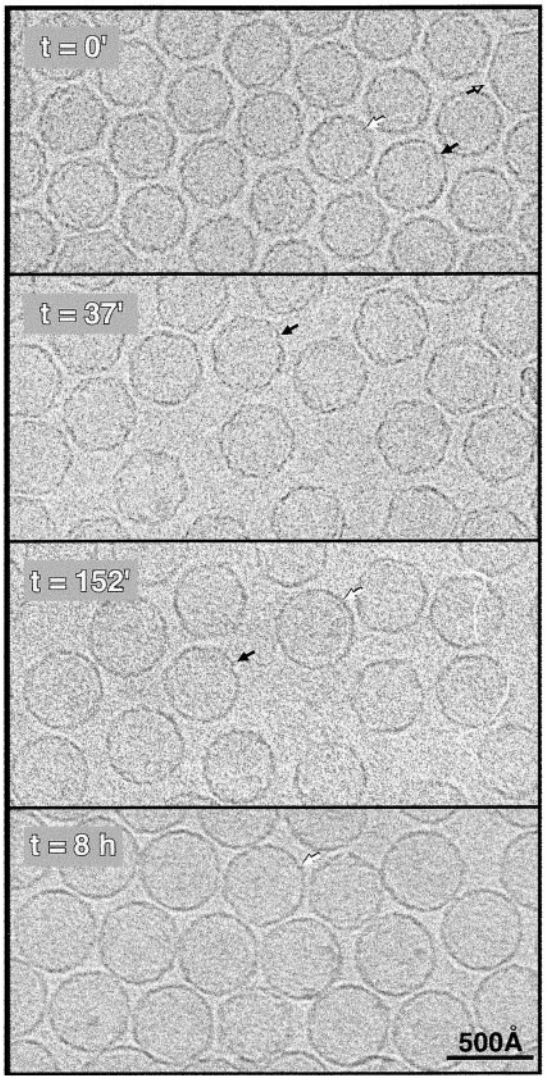

Figure 3. Cryo-Micrographs of HK97 Capsids from Successive Time Points of an Acid-Induced Maturation Experiment

The starting material (t = 0) was >95% Prohead II: white arrow—a typical particle. Also present were a few partially expanded, i.e., E-I/II–like, particles—black arrow, and Heads—hollow black arrow. The 37 min sample was mainly E-I, and the 152 min sample, mainly E-II (see Figure 6 and Results): black arrows mark typical particles. At 152 min, there were few E-III particles (e.g., white arrow), but they became the majority species at 8 hr.

Structural Changes in the Expansion Intermediates

Three-dimensional density maps were calculated to resolutions of 20–27 Å (cf. Table 1) for each of the novel species of particles characterized E-I, E-II, and E-III. In addition, we reconstructed Prohead II to higher resolution (17 Å) than before (cf. the 25 Å map of Conway et al., 1995). These structures are compared in Figure 4. During these studies, we determined the handedness of Prohead II by means of the tilting method of Belnap

Table 1. Electron Density Maps—Summary

Particle	Number of Particles	Resolution	% Increase in Internal Volume	% Increase in Diameter as Measured Along[c]		
				2-Fold Axis	3-Fold Axis	5-Fold Axis
Prohead II	408	17 Å	—	—	—	—
E-I	345	20 Å	38[b]	11	8	10
E-II	346	24 Å	44[b]	13	14	10
E-III	126	27 Å	86	25	25	13
Head[a]	65	25 Å	102	25	25	20

[a] From Conway et al. (1995). This map was reconstructed using particles from a single micrograph and was not CTF corrected.
[b] Uncertainty in internal volume (±1%) reflects a correction applied to E-II because the correct contour level (corresponding to 100% of expected mass) resulted in holes on the surface.
[c] Diameters were measured manually along the respective axes. Estimated uncertainties are ±1%. Increases are relative to Prohead II.

et al. (1997), finding its T = 7 surface lattice to be the *laevo* enantiomorph. Thus, the handedness provisionally assigned by Conway et al. (1995) on grounds of the "lambdoid" character of HK97, the lambda capsid having been reported to be T = 7 *laevo* (Bayer and Bocharov, 1973), was confirmed.

When Prohead II converts to E-I, the most pronounced structural change is that the hexon asymmetry—strongly expressed on the outer surface of Prohead II—is largely obviated (cf. Figure 4): moreover, the pentons change perceptibly, as manifested by an apparent slight rotation about their symmetry axis. Central sections (cf. Figures 5a and 5b) illustrate the extent to which the surface profile has flattened in this transition.

E-I and E-II are very similar in size but structurally distinct (cf. Figure 4). The E-II penton protrusions appear to have shrunk and rotated relative to those of E-I, and the hexons have levelled out further and become rotund: also, the surface relief has further flattened, as is most evident on the inner surface.

Although the round shape and bland appearance of the balloon-like E-III particle made the determination of orientations more difficult, we eventually obtained a reconstruction of similar resolution to those of E-I and E-II. In the E-III map, the penton protrusions have altered little compared to their disposition in E-II, but the outer surface relief of the hexons is now barely discernible (cf. Figure 4). Nevertheless, the hexons are still quasi-globular in shape and have not yet taken on the sharply expressed 6-fold symmetry of hexons on Heads. A central section through E-III (Figures 5c and 5d) reveals its round, even, surface contour, and comparison with sections through E-I and E-II accentuates its significantly increased diameter. The dimensions of these particles are compared in Table 1.

Half-Lives of Subtransitions on the Acid-Induced Maturation Pathway

The particle populations imaged at each time point were sorted into four classes: Prohead II and the three Expansion Intermediates. Although there were always a few Heads present, they did not increase perceptibly in numbers until the preparation was switched to neutral pH and so were ignored in our analysis of the intervening time points. When present, Prohead II and E-III were readily recognized on grounds of their distinctive sizes and shapes. E-I and E-II have much the same size and general appearance and were distinguished by correlation analysis (Experimental Procedures).

The prevalence of each class as a function of time is summarized in Figure 6a. The starting population consisted almost exclusively of Prohead II. By the first time point sampled (5 min), none of the 1251 particles counted could be convincingly identified as Prohead II: all were 8%–10% larger, implying that this conversion is rapid. Modeling this event with first order kinetics, these data imply an upper limit of <30 s for the half-life of Prohead II at pH 4.18. Thereafter, the distributions document a gradual conversion to E-II and, subsequently, to E-III (Figure 6a). To estimate the longevity of these species, these data (the percentages of the 3 Expansion Intermediates at each of 10 time points) were modeled using first order kinetics. This calculation yielded an estimated half-life of 119 min for the E-I → E-II transition and 103 min for the E-II → E-III transition. At pH 4.18, E-III represented the endstate. However, on reverting to pH 7, these particles gradually assumed the angular morphology of Head II.

Is E-III an Intermediate at Physiological pH? The Acid-Pulse Pathway

Although E-III is the endstate of acid-induced expansion, both the X-ray and the cryo-EM data indicate that E-III particles accumulated at pH ∼4 will convert to Heads if restored to neutrality. Nevertheless, the question remains whether E-III is a bona fide on-pathway intermediate or an artifact of acidic pH. To address this, we performed the acid-pulse experiment. After 30 min at pH 4.18, when all particles were E-I or E-II, they were switched to pH 7. Would they proceed to the Head state directly or via an E-III intermediate?

Cryo-micrographs were recorded at the times indicated in Figure 6b, and the particles were classified as described above. As a control, part of the preparation was kept at pH 4.18, and its eventual status as E-III was confirmed. At the 60 min time point, 77% of the acid-pulsed particles were still E-I or E-II, and the rest were either visibly angular Heads or round, thin-walled particles of much the same size. By the 90 min time point, all particles were of the latter type, apart from 10%–15% that had reverted to the Prohead II state (confirmed as such, by image reconstruction). The same populations persisted at 20 hr (Figure 6b), and we conclude that a subclass of E-I-sized particles are capable of reverting to the Prohead II state. This was the only example that we encountered of movement along the maturation pathway that was not irreversible.

In principle, the round, thin-walled particles observed

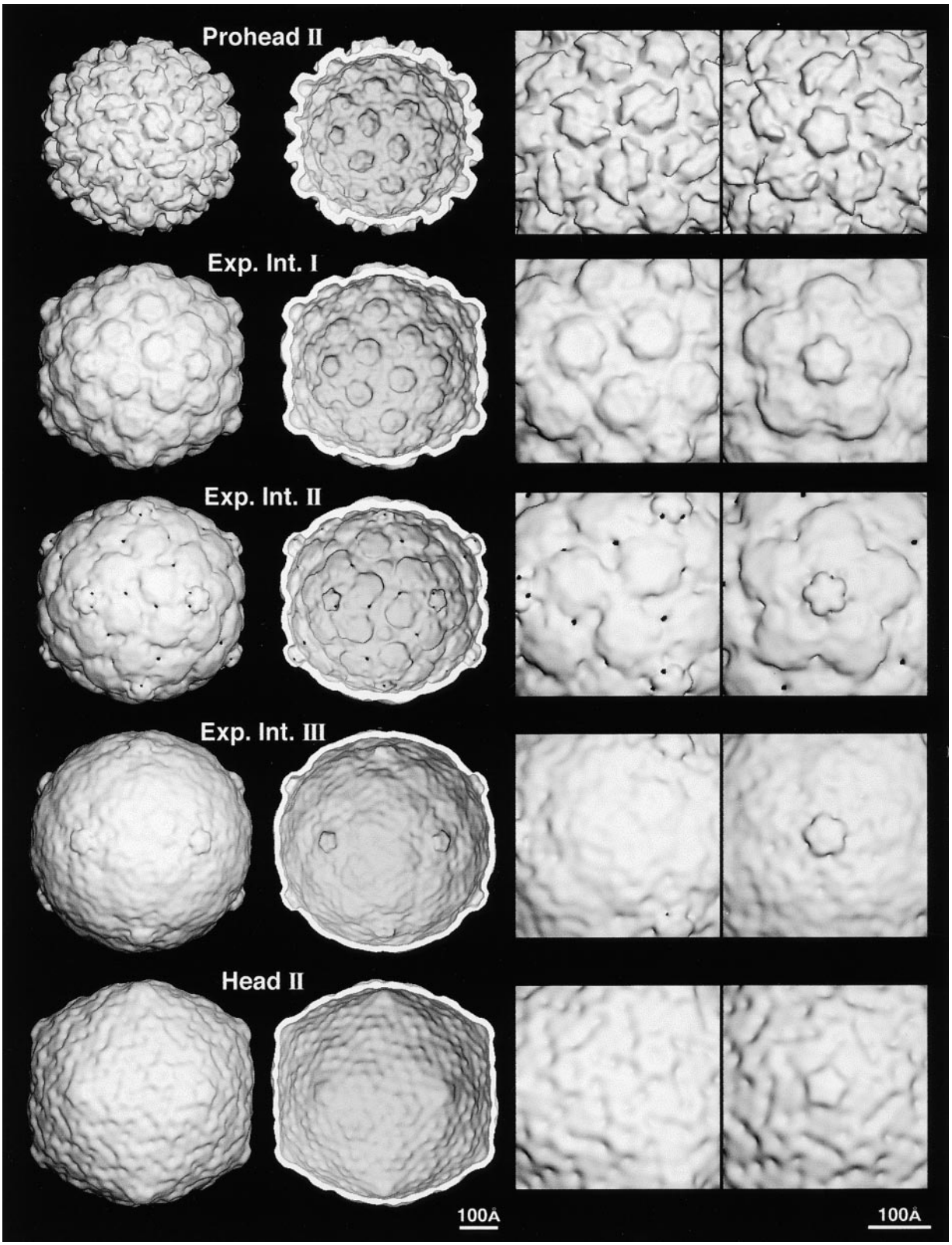

Figure 4. Three-Dimensional Reconstructions of the HK97 Capsid at Successive Stages of Maturation

Comparison of the three-dimensional structures of Prohead II; Expansion Intermediates I, II, and III; and Head II (from Conway et al., 1995). Column 1, outer surface; column 2, inner surface. Also shown are blow-ups of capsid features around the 3-fold (column 3) and 5-fold (column 4) symmetry axes. The reconstructions were rendered so as to enclose 100% of expected mass.

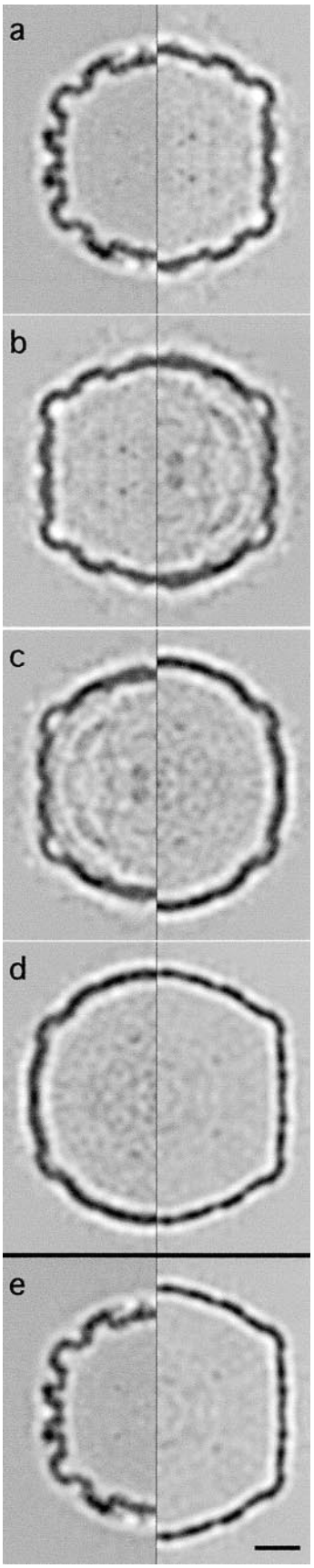

at 60 min and later could be either Heads viewed close to a 5-fold symmetry axis or E-III, which appears round from any direction. To resolve this ambiguity, all such particles from the 60 min and 90 min time points were matched with reprojections of both the E-III and the Head maps and classified on the basis of the resulting correlation coefficients. This analysis indicated that a few particles, ~2% of the 60 min population and ~1% of the 90 min population, were E-III. These identifications were confirmed by visually comparing the corresponding reprojections and micrographs (data not shown). Thus, we conclude that E-III is indeed an intermediate, albeit a short-lived one, on the neutral pH pathway.

Dynamic Visualization of Capsid Expansion

To better apprehend the complex sequence of movements that take place in the expansion transformation, we integrated the seven reconstructions from Prohead II through Head II into a movie (see Dynamic Visualization in Experimental Procedures). This visualization technique has been used to advantage to convey the various nucleotide-binding states of the molecular chaperone, GroEL (White et al., 1997). Here we have enhanced it by including the graphic technique of morphing to connect frames, thus showing the transitions between successive capsid conformations in a more continuous manner.

Discussion

Molecular Behavior of Capsid Maturation

The phenomenon of capsid maturation is widespread and perhaps universal among dsDNA phages. It also occurs in dsRNA phages (Butcher et al., 1997) as well as for some animal viruses that assemble a precursor prior to DNA packaging. Herpesviruses fall into this category (Newcomb et al., 1996; Trus et al., 1996). Maturation is also a feature of retrovirus replication, although in this case, the packing of Gag proteins in the precursor particle may not be icosahedral (Fuller et al., 1997; Yeager et al., 1998; but see Nermut et al., 1998).

Despite substantial diversity in the sizes, sequences, and numbers of capsid proteins, maturation exhibits some generic features that are common to all bacteriophages and herpesviruses characterized to date. The procapsid shell is round, relatively fragile, and its hexons show marked departures from 6-fold symmetry. The mature capsid is angular, relatively robust, and has symmetric hexons. Maturation takes place as a coordinated event on a given particle and is irreversible. Unlike cyclic conformational changes in the force-generating cycles of motor proteins that are powered by nucleotide hydrolysis (Cooke, 1995), capsid maturation represents the

Figure 5. Successive Stages of HK97 Prohead II Maturation

Each particle is compared with the subsequent state in half-plane juxtapositions of central sections through the respective density maps. On account of symmetry, a half-plane section contains full information. The sections are from maps viewed along a 2-fold symmetry axis. (a) Prohead II on left (L) versus E-I on right (R); (b) E-I (L) versus E-II (R); (c) E-II (L) versus E-III (R); (d) E-III (L) versus Head (R); and lastly, the endpoints, (e) Prohead II (L) versus Head (R). Bar = 100 Å.

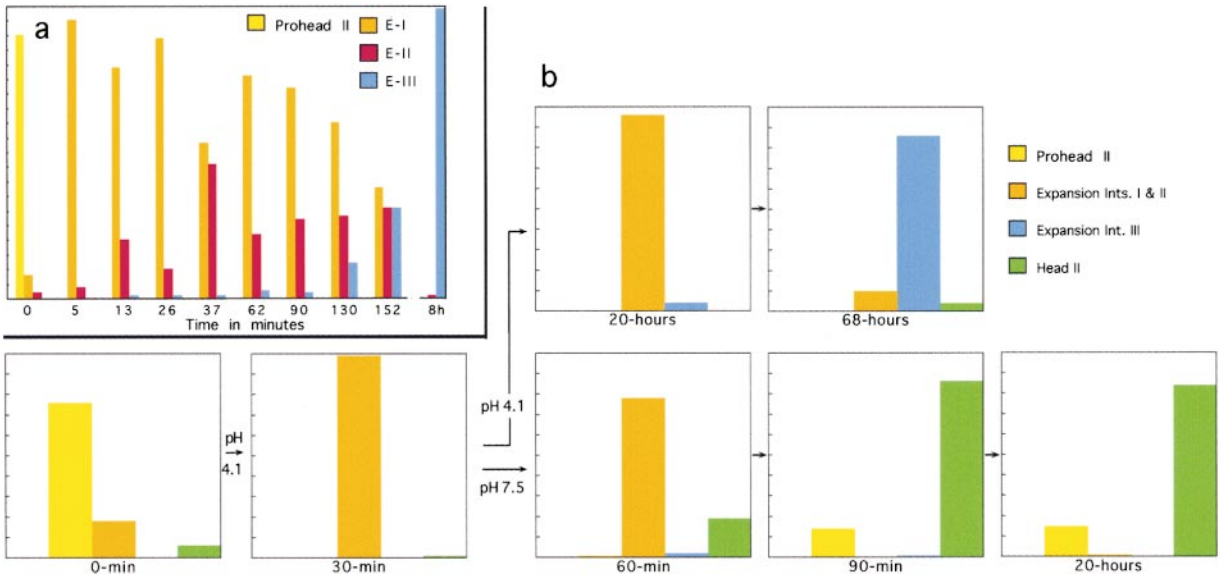

Figure 6. Time Course of the Appearance and Disappearance of Various Particle Species in HK97 Capsid Maturation In Vivo

Histograms plotting the time courses of (a) an acid-induced expansion experiment, in which the pH was dropped from 7 to 4.18 at t = 0 min—note the break between the 152 min and 8 hr time points; and (b) an acid-pulse expansion experiment that was initiated in the same way but part of the sample (bottom branch) was restored to pH 7 after 30 min. The proportions of different particle species at each time point were determined by counting from cryo-micrographs. Full scale = 100%.

transition from one local minimum of conformational free energy to another, lower and exothermic, minimum (Steven et al., 1992; Galisteo and King, 1993). As such, intermediate states in capsid maturation are formally equivalent to staging posts in protein-folding pathways and are thus directly germane to this fundamental field of study (Tuma et al., 1998).

Originally observed by negative staining and thin sectioning, capsid maturation has now been characterized by cryo-microscopy for bacteriophages lambda (Dokland and Murialdo, 1993), P22 (Prasad et al., 1993), HK97 (Conway et al., 1995), PRD1 (Butcher et al., 1997), and ϕ29 (Tao et al., 1998). The HK97 system has properties that facilitate the investigation of dynamic aspects of maturation (see Introduction).

Consistency of Experimental Approaches

The cryo-EM and X-ray diffraction experiments were designed on the basis of prior work by agarose gel electrophoresis, which distinguished two populations of particles that migrate with the mobilities of Prohead II and Head, respectively (e.g., Figure 2a). In addition, they indicated a half-life for expansion of ~30 min at pH 4.18. Subsequent cryo-EM analysis indicated that conversion took much longer at this pH, that long-lived intermediates were present, and that the endpoint was E-III, not Head. However, these observations are not in contradiction. Because the gels were run at pH ~8, these were "acid-pulse" experiments, whose endpoint is indeed Head II. Thus, although we do not yet know whether the Expansion Intermediates have distinctive net surface charges, i.e., electrophoretic mobilities, we may conclude that the two lines of evidence are consistent. And the agarose gel experiments succeeded in defining conditions under which expansion might usefully be probed by time-resolved X-ray diffraction and cryo-EM.

Maturation was monitored by X-ray diffraction under slightly more acidic conditions than in the cryo-EM experiments (pH 4.0 versus 4.18), which would be expected to accelerate conversion and such proved to be the case. The endpoint spectrum turned out to be significantly different from that of Head II, and cryo-EM showed that it corresponded to the E-III particle. The evolution of the spectrum with time was modeled in terms of a one-step process for particles of two different sizes. These data yielded a half-life of ~10 min, as compared to ~4 hr at pH 4.18, according to cryo-EM. Here, we infer that the modeled transition represents conversion of mixed populations of Prohead II, E-I, and E-II (which should have relatively similar powder patterns) to E-III (which is larger and thinner walled and should have a distinct spectrum). Thus, these two lines of experimentation are also consistent and mutually complementary.

Homogeneity of Populations

Our analysis of the cryo-EM data is based on the inference that maturing HK97 capsids exist in several discreet, icosahedrally symmetric, states. This scenario is likely an oversimplification, and it may well be that maturing populations also contain particles that are not icosahedrally symmetric—i.e., they have capsomers in multiple conformations, and there are other subtly different icosahedrally symmetric states. This proposition may be addressed by employing more powerful classification techniques than we have used so far, and such analysis will be key to distinguishing additional transitional states (if they exist) from cryo-EM data and to extending the resolution of our three-dimensional models. Nevertheless, the resolutions of current reconstructions—17 to 25 Å—suggest that the placement of proteins within them is consistent to within excursions of

~4–6 Å (Conway and Steven, 1999). Moreover, at all time points, the majority of particles that were not Prohead II or Head could be accounted for as one of the three currently recognized intermediates. These considerations suggest that the present scenario represents a good first approximation to the acid-induced maturation pathway.

Kinetics of Expansion

The data currently on hand suggest that capsids expanding in vitro under different conditions progress through the same set of intermediates but may spend widely differing times in a given state. For instance, Prohead II stored at pH 7 registers only very low levels of spontaneous maturation, as evidenced by the small amounts of E-I/II–sized particles and Heads present in our starting material and in other such preparations that we have examined. In particular, the Prohead II → E-I conversion is very slow under these conditions, whereas it is rapid (<30 s) at pH 4.18. Conversely, at pH 4.18, E-III remains indefinitely in this state, but is very short-lived at pH 7.

Thus, we think of capsid expansion as progression through a series of conformational intermediates for which the relative energetic status—and consequently their rates of interconversion—can be strongly influenced by the environment. The stability of E-III at acidic pH and its rapid conversion to Head upon neutralization is perhaps the clearest example of this. Progress along the pathway appears to be irreversible, excepting the first step in that an environmental change (raising the pH) in the acid-pulse experiment resulted in the reappearance of significant amounts of Prohead II in a population that contained no such particles at the time of neutralization. A similar interpretation can be made of the agarose gel results. It is an attractive, though untested, possibility that changes in the local environment of the protein subunits might serve to drive capsid maturation forward through otherwise energetically unfavorable transitions, i.e., kinetic barriers to maturation. Thus, insertion of DNA into Prohead II during packaging might amount to a change that switches the status of the Prohead II to E-II transition from energetically unfavorable to favorable, just as seems to be the case upon acidification of Prohead II in vitro.

And how does maturation proceed in vivo? Capsid expansion is a relatively early event in DNA packaging and thus requires less time than packaging, for which 1.8 min has been estimated for phage T3 at 30° (Shibata et al., 1987), a number that may also apply to HK97 with its similarly sized genome. If expansion is initiated after ~25% of the genome has entered the capsid as in T3 (Shibata et al., 1987) and lambda (Hohn, 1983) and is complete at, say, 50%, these considerations would place an upper bound of ~30 s for expansion. However, in vivo, with the growing pressure imposed on the inner capsid surface by incoming DNA, it may be much faster.

Making Waves: Is the Connector/Portal the Expansion Epicenter?

At the outset, we envisaged two general mechanisms for expansion: a series of relatively minor subtransitions, and a single major transition initiated locally and propagating as a wavefront over the surface lattice. The Expansion Intermediates observed in this study are in line with the former expectation, whereas maturation waves have been observed directly on elongated variants of the T4 capsid (Steven and Carrascosa, 1979; Müller et al., 1994). However, there are significant differences between the respective systems. To date, propagating waves have been observed only with cylindrical surface lattices, not on closed icosahedral particles, where the presence of vertices may impede the development of a coherent wavefront (see Jardine and Coombs, 1998). The second difference is that the HK97 capsids studied here lack the connector/portal protein via which DNA enters and leaves the capsid and that also initiates procapsid assembly in some systems (Valpuesta and Carrascosa, 1994). Although the absence of the connector facilitates structural analysis, in that all twelve vertices averaged in density maps are intrinsically alike instead of having a singular vertex occupied by the connector, these particles are nonnative in the sense that they cannot be packaged. The observation that T7 procapsids are more prone to expansion if they contain a connector (M. E. Cerritelli et al., personal communication) suggests the possibility that conformational changes in this protein are transmitted to neighboring capsid protein subunits and thence to their neighbors, and so on, thus generating a transition wave with the connector at its epicenter. Nevertheless, it remains possible that, in the maturing HK97 capsid, there are at least three such waves, associated with the conformations of Expansion Intermediates I, II, and III, respectively. Further work involving cryo-EM of maturing connector-containing Proheads may help to clarify this question.

Nature of the Conformational Changes

In our perception, the movie (see Dynamic Visualization) provides the best medium for conveying the flow of density that remodels the maturing surface lattice. The Expansion Intermediates reveal that the first major feature of Prohead II to change is the hexon shear that divides this capsomer into a pair of nonequivalent trimers. Already in E-I, this asymmetry is largely eliminated (cf. Figure 4). Thereafter, the shape of the hexon continues to evolve, and only assumes the near-perfect 6-fold symmetry of its Head conformation at a late stage, i.e., post E-III.

During expansion, the penton protrusions appear to rotate through ~35° about their symmetry axis, and to change in size and shape (Figure 4). At present, we cannot distinguish between the following possibilities: (1) preserved subunit or domainal structures undergo some more general rotational displacement(s), which at the current resolution resemble an axial rotation and net shrinkage of the protruding portion of the penton; or (2) in addition to rigid-body movements, the transition also involves a significant amount of refolding. The latter mechanism has been documented in the T4 and P22 systems by the detection of significant changes in secondary structure between the precursor and mature conformations (Steven et al., 1990; Tuma et al., 1996). For HK97 Head II, a high resolution crystal structure has now been determined (Wikoff et al., 1998; 1999; and

unpublished data). This information, in conjunction with the cryo-EM density maps of the Expansion Intermediates, should allow us to address the molecular mechanics of capsid expansion in greater detail.

Experimental Procedures

Particle Preparation and Agarose Gel Electrophoresis

Prohead II was produced using an efficient expression plasmid (pT7-Hd2.9) and purified using precipitation, sedimentation, and ion-exchange chromatography, essentially as described (Duda et al., 1995a; Duda, 1998). These particles do not contain the connector/portal protein that is not essential for morphogenesis in the HK97 system (Xie and Hendrix, 1995). Preparations were stored at 4°C at protein concentrations of 14.6–16 mg/ml in 20 mM Tris HCl, 250 mM KCl, pH 7.52, and used for structural analysis within a few days. Head II was produced and purified as described by Duda et al. (1995a and b) and stored at 4°C at 46 mg/ml in the same buffer, plus 1 mM 2-mercaptoethanol. Samples were electrophoresed in nondenaturing 1.2% agarose gels, as described by Duda et al. (1995a), following Serwer and Pichler (1978), except for different buffers, running conditions, and staining methods.

Low-Angle X-Ray Scattering

Solution scattering data were collected at Stanford Synchrotron Radiation Laboratory (SSRL) beamline 4–2 (Tsuruta et al., 1998) at a wavelength of 1.488 Å, using a linear BioLogic/EMBL model 210 detector at a sample-to-detector distance of 2.3 m to cover the range of ~700 Å to ~30 Å. Data were collected at 22°C, using a 40 μl polycarbonate sample cell with 20 μm thick mica windows. For each sample, a buffer spectrum, recorded first and normalized to the primary beam intensity, was subtracted from its scattering curve. "Static" scattering curves were measured for Prohead II (16 mg/ml) and Head II (46 mg/ml), in each case averaging over five 3 min exposures.

Expansion was induced by adding 1/10 vol of 1 M NaAcetate, pH 4.0. The time lag between mixing and the first data point ($t = 1'$) was 60 s. Scattering curves were then recorded with 1 min exposures, at 1 min intervals, for 30 min. In one experiment, after 30 min, the sample was removed from the cuvette, neutralized by mixing with 8 μl of 1M Tris-HCl, pH 8.3, returned to the cuvette 10 min later, and then remeasured.

The data were analyzed in terms of models consisting of spherical shells of constant density. Their radii were determined by calculating scattering curves for shells with a wide range of inner and outer radii and optimizing the fit to the data, and selecting the model that gave the highest correlation with the data. In these comparisons, the scattering curves were weighted as the cube of the resolution, *s*. In each comparison, an optimal linear scale factor between calculated and experimental data was determined and applied.

Time-Resolved Cryo–Electron Microscopy

The $t = 0$ control sample was prepared by diluting a Prohead II preparation 8-fold in storage buffer to 1.8 mg/ml protein, and then applying a 5 μl droplet to a holey carbon film, blotting to a thin film, and vitrifying as described by Conway et al. (1995). Shortly thereafter, another portion of the same preparation was diluted by the same factor and simultaneously acidified to pH 4.18 by adding an appropriate volume of 0.2 M KCl buffered with 50 mM sodium acetate, pH 4.109 (pH was measured with a Corning Ion Analyzer Model 250). In the acid-induced maturation experiment reported in detail above, the preparation was first sampled at 5 min and then at progressively longer intervals until 48 hr, when the pH was restored to 7.0. The final sample was taken 20 hr later. In all, 13 grids were prepared. In each case, a 5 μl drop was abstracted from the sample and used to prepare a grid, as above. These grids were stored under liquid N_2 until they could be examined (up to 48 hr). Specimens were observed on a Philips CM200-FEG electron microscope (FEI, Mahwah, NJ) operated at 120 keV and a magnification of 38,000, using low-dose techniques. Numerous focal pairs, the first zeros of whose contrast transfer functions (CTF) were at frequencies of ~(20 Å)$^{-1}$ and ~(25 Å)$^{-1}$, respectively, were recorded for each time point. Essentially the same procedure was followed in analyzing the acid-pulse pathway.

Image Analysis and Three-Dimensional Image Reconstruction

Micrographs were digitized on a Phodis scanner (Zeiss Photogrammetrics, Englewood, CO) at 7 μm per pixel, then these data were binned to give 14 μm sampling (3.7 Å at the specimen). Particle images were extracted and preprocessed as described by Conway et al. (1993) and Conway and Steven (1999). In general, reconstructions were calculated as reviewed by Fuller et al. (1996), using the PFT algorithm of Baker and Cheng (1996) to determine particle orientations. Since our main goal—to identify specific intermediates along the expansion pathway—required the calculation of many reconstructions, the analysis was initially confined to particles from single micrographs rather than focal pairs (Zlotnick et al. 1996; Conway et al., 1997; Trus et al., 1997). The further-from-focus members of focal pairs, having higher contrast, were used for this purpose, and this analysis was restricted to a resolution of ~25 Å. Subsequently, focal pairs were combined and CTF corrected as described by Zlotnick et al. (1996) and Conway et al. (1997). Details of the final reconstructions are listed in Table 1. Resolutions of the maps were assessed in terms of the Fourier Shell Correlation (FSC) criterion (Saxton and Baumeister, 1982).

Our strategy for identifying homogeneous subsets of particles, each representing a relatively stable intermediate, is described below. Micrographs from 10 time points were analyzed in detail. All particles that were not visibly damaged or otherwise compromised were classified according to size, then subclassified on the basis of structure. Size discrimination was performed by comparing each particle with variously scaled copies of a common model and assigning it to the size class that gave the largest real-space correlation coefficient (Baker and Cheng, 1996). Data from the 37 min time point were analyzed first, because these particles were relatively uniform in size. The Prohead II map of Conway et al. (1995) was rescaled appropriately and used as a starting model to calculate a density map at ~25 Å resolution (model 37A) that included all particles with correlation coefficients greater than the average for the data set. For all other time points analyzed, reference models ranging in size from 0%–18% larger than Prohead II in increments of 2% were tried. Suitably scaled versions of Prohead II were used to cover the increment range of 0%–8% and of model 37A for the range of 10%–18%. After orientation determination with PFT, each particle was assigned to the size class of the model that gave the highest correlation coefficient.

To classify by structure, reconstructions were initially calculated for each size class at each time point. Since these maps were based on relatively small sets of particles, reconstructions were also calculated from larger sets, including particles from both adjacent size classes, i.e., ±2% in scaling. These reconstructions were assessed visually for similarities and differences, and data from different time points that produced like models were pooled to form a new set of reference structures. The process was then repeated. In each cycle, this analysis was repeated, each particle being compared to each current model and assigned on the basis of the highest correlation coefficient (Baker and Cheng, 1996). For this purpose, we used the average of the three correlation coefficients calculated in PFT, but the outcome was not sensitive to this particular choice, as confirmed by trials with particles of known identity. The final reconstructions included all particles whose correlation coefficients were greater than the average value minus one half-standard deviation (i.e., the top ~40% in each class).

Mathematical Modeling of Kinetics

At each time point, the percentages of particles of each kind were identified as described above. These data were modeled, assuming first order kinetics for each transition. The rate constants were determined by a least-squares fit using the function *FindMinimum* in MATHEMATICA (Wolfram Research Inc.), and converted to half-lives. For the first time point (5 min), an upper bound for the half-life of Prohead II at pH 4.18 was obtained on the basis of there being a maximum of one such particle surviving at this time point.

Dynamic Visualization

The dynamic progression of expansion was represented in a movie (available at http://www.cell.com/cgi/content/full/100/2/253/DC1)

in which surface renderings of experimental density maps were interspersed with "morphed" images to provide a visually smooth transition at each stage. The morphed frames were generated with the Morph 2.5 software package (Gryphon Software Corp, San Diego, CA). For each step, corresponding features on the respective surface renderings of the initial and final state maps were identified by hand as a series of control points and edges. A sequence of images was then generated by geometrically warping the initial and final views to generate successive steps in the transition, and combining the warped images with suitable weighting. The transition sequences thus generated were assembled into movie "clips" and, finally, a complete movie, using Adobe Premier 5.1 (Adobe Systems, Inc, Mountain View, CA). A color transition was superimposed on the movie, and text was added at this stage. This process was followed twice—once for exterior views and once for interior views. The final movie file is in QuickTime format. All processing, including output to videotape, was performed on a PowerMac 8500 (Apple, Cupertino, CA).

Acknowledgments

We thank D. R. Humphrey for excellent technical assistance in purifying Prohead II and refining the expansion conditions, Drs. D. Belnap and B. Trus for helpful discussions, and Dr. D. Winkler for help with graphics. This work was supported in part by NIH grant R01 GM47795 (RWH). Experiments at the SSRL were supported by NIH grants R01 AI40101 (JEJ), P41 RR01209 (SSRL), and the Department of Energy.

Received November 8, 1999; revised December 10, 1999.

References

Baker, T.S., and Cheng, R.H. (1996). A model-based approach for determining orientations of biological macromolecules imaged by cryoelectron microscopy. J. Struct. Biol. *116*, 120–130.

Bayer, M.E., and Bocharov, A.F. (1973). The capsid structure of bacteriophage lambda. Virology *54*, 465–475.

Belnap, D.M., Olson, N.H., and Baker, T.S. (1997). A method for establishing the handedness of biological macromolecules. J. Struct. Biol. *120*, 44–51.

Berriman, J., and Unwin, N. (1994). Analysis of transient structures by cryo-microscopy combined with rapid mixing of spray droplets. Ultramicroscopy *56*, 241–252.

Butcher, S.J., Dokland, T., Ojala, P.M., Bamford, D.H., and Fuller, S.D. (1997). Intermediates in the assembly pathway of the double-stranded RNA virus phi6. EMBO J. *16*, 4477–4487.

Conway, J.F., and Steven, A.C. (1999). Methods for reconstructing density maps of "single particles" from cryoelectron micrographs to subnanometer resolution. J. Struct. Biol. *128*, 106–118.

Conway, J.F., Duda, R.L., Cheng, N., Hendrix, R.W., and Steven, A.C. (1995). Proteolytic and conformational control of virus capsid maturation: the bacteriophage HK97 system. J. Mol. Biol. *253*, 86–99.

Conway, J.F., Cheng, N., Zlotnick, A., Wingfield, P.T., Stahl, S.J., and Steven, A.C. (1997). Visualization of a 4-helix bundle in the hepatitis B virus capsid by cryo–electron microscopy. Nature *386*, 91–94.

Cooke, R. (1995). The actomyosin engine. FASEB J. *9*, 636–642.

Dokland, T., and Murialdo, H. (1993). Structural transitions during maturation of bacteriophage lambda capsids. J. Mol. Biol. *233*, 682–694.

Duda, R.L. (1998). Protein chainmail: catenated protein in viral capsids. Cell *94*, 55–60.

Duda, R.L., Hempel, J., Michel, H., Shabanowitz, J., Hunt, D., and Hendrix, R.W. (1995a). Structural transitions during bacteriophage HK97 head assembly. J. Mol. Biol. *247*, 618–635.

Duda, R.L., Martincic, K., and Hendrix, R.W. (1995b). Genetic basis of bacteriophage HK97 prohead assembly. J. Mol. Biol. *247*, 636–647.

Flynn, D.L., Abood, N.A., and Holwerda, B.C. (1997). Recent advances in antiviral research: identification of inhibitors of the herpesvirus proteases. Curr. Opin. Chem. Biol. *1*, 190–196.

Fuller, S.D., Butcher, S.J., Cheng, R.H., and Baker, T.S. (1996). Three-dimensional reconstruction of icosahedral particles—the uncommon line. J. Struct. Biol. *116*, 48–55.

Fuller, S.D., Wilk, T., Gowen, B.E., Krausslich, H.G., and Vogt, V.M. (1997). Cryo-electron microscopy reveals ordered domains in the immature HIV-1 particle. Curr. Biol. *7*, 729–738.

Galisteo, M.L., and King, J. (1993). Conformational transformations in the protein lattice of phage P22 procapsids. Biophys. J. *65*, 227–235.

Hendrix, R.W., and Duda, R.L. (1998). Bacteriophage HK97 head assembly: a protein ballet. Adv. Virus Res. *50*, 235–288.

Hohn, B. (1983). DNA sequences necessary for packaging of bacteriophage lambda DNA. Proc. Natl. Acad. Sci. USA *80*, 7456–7460.

Jardine, P.J., and Coombs, D.H. (1998). Capsid expansion follows the initiation of DNA packaging in bacteriophage T4. J. Mol. Biol. *284*, 661–672.

King, J., and Chiu, W. (1997). The procapsid-to-capsid transition in double-stranded DNA bacteriophages. In Structural Biology of Viruses, W. Chiu, R.M. Burnett, and R. Garcea, eds. (New York: Oxford University Press), pp. 288–311.

Müller, M., Mesyanzhinov, V., and Aebi, U. (1994). In vitro maturation of prehead-like bacteriophage T4 polyheads: structural changes accompanying proteolytic cleavage and lattice expansion. J. Struct. Biol. *112*, 199–215.

Nermut, M.V., Hockley, D.J., Bron, P., Thomas, D., Zhang, W.H., and Jones, I.M. (1998). Further evidence for hexagonal organization of HIV gag protein in prebudding assemblies and immature virus-like particles. J. Struct. Biol. *123*, 143–149.

Newcomb, W.W., Homa, F.L., Booy, F.P., Thomsen, D.R., Trus, B.L., Steven, A.C., Spencer, J.V., and Brown, J.C. (1996). Assembly of the herpes simplex virus capsid: characterization of intermediates observed during cell-free capsid formation. J. Mol. Biol. *263*, 432–446.

Prasad, B.V.V., Prevelige, P.E., Marietta, E., Chen, R.O., Thomas, D., King, J., and Chiu, W. (1993). Three-dimensional transformation of capsids associated with genome packaging in a bacterial virus. J. Mol. Biol. *231*, 65–74.

Saxton, W.O., and Baumeister, W. (1982). The correlation averaging of a regularly arranged bacterial cell envelope protein. J. Microsc. *127*, 127–138.

Serwer, P., and Pichler, M.E. (1978). Electrophoresis of bacteriophage T7 and T7 capsids in agarose gels. J. Virol. *28*, 917–928.

Shibata, H., Fujisawa, H., and Minagawa, T. (1987). Characterization of the bacteriophage T3 DNA packaging reaction in vitro in a defined system. J. Mol. Biol. *196*, 845–851.

Steven, A.C., and Carrascosa, J.L. (1979). Proteolytic cleavage and structural transformation: their relationship in bacteriophage T4 capsid maturation. J. Supramol. Struct. *10*, 1–11.

Steven, A.C., Greenstone, H., Bauer, A.C., and Williams, R.W. (1990). The maturation-dependent conformational change of the major capsid protein of bacteriophage T4 involves a substantial change in secondary structure. Biochemistry *29*, 5556–5561.

Steven, A.C., Greenstone, H.L., Booy, F.P., Black, L.W., and Ross, P.D. (1992). Conformational changes of a viral capsid protein: Thermodynamic rationale for proteolytic regulation of bacteriophage T4 capsid expansion, cooperativity, and super-stabilization by *soc* binding. J. Mol. Biol. *228*, 870–884.

Tao, Y., Olson, N.H., Xu, W., Anderson, D.L., Rossmann, M.G., and Baker, T.S. (1998). Assembly of a tailed bacterial virus and its genome release studied in three dimensions. Cell *95*, 431–437.

Trus, B.L., Booy, F.P., Newcomb, W.W., Brown, J.C., Homa, F.L., Thomsen, D.R., and Steven, A.C. (1996). The herpes simplex virus procapsid: structure, conformational changes upon maturation, and roles of the triplex proteins VP19c and VP23 in assembly. J. Mol. Biol. *263*, 447–462.

Trus, B.L., Roden, R.B.S., Greenstone, H.L., Schiller, J.T., and Booy, F.P. (1997). Novel structural features of bovine papillomavirus capsid

revealed by a three dimensional reconstruction to 9Å resolution. Nat. Struct. Biol. *4*, 413–420.

Tsuruta, H., Brennan, S., Rek, Z.U., Irving, T.C., Tompkins, W.H., and Hodgson, K.O. (1998). A wide-bandpass multilayer monochromator for biological small-angle scattering and fiber diffraction studies. J. Appl. Crystallogr. *31*, 672–682.

Tuma, R., Prevelige, P.E., Jr., and Thomas, G.J., Jr. (1996). Structural transitions in the scaffolding and coat proteins of P22 virus during assembly and disassembly. Biochemistry *35*, 4619–4627.

Tuma, R., Prevelige, P.E., Jr., and Thomas, G.J., Jr. (1998). Mechanism of capsid maturation in a double-stranded DNA virus. Proc. Natl. Acad. Sci. USA *95*, 9885–9890.

Valpuesta, J.M., and Carrascosa, J.L. (1994). Structure of viral connectors and their function in bacteriophage assembly and DNA packaging. Q. Rev. Biophys. *27*, 107–155.

Walker, M., Trinick, J., and White, H. (1995). Millisecond time resolution electron cryo-microscopy of the M-ATP transient kinetic state of the acto-myosin ATPase. Biophys. J. *68*, 87S–91S.

White, H.E., Chen, S., Roseman, A.M., Yifrach, O., Horovitz, A., and Saibil, H.R. (1997). Structural basis of allosteric changes in the GroEL mutant Arg197 → Ala. Nat. Struct. Biol . *4*, 690–694.

Wikoff, W.R., Duda, R.L., Hendrix, R.W., and Johnson, J.E. (1998). Crystallization and preliminary X-ray analysis of the dsDNA bacteriophage HK97 mature empty capsid. Virology *243*, 113–118.

Wikoff, W.R., Duda, R.L., Hendrix, R.W., and Johnson, J.E. (1999). Crystallographic analysis of the dsDNA bacteriophage HK97 mature empty capsid. Acta Crystallogr. D *55*, 763–771.

Wlodawer, A., and Erickson, J.W. (1993). Structure-based inhibitors of HIV-1 protease. Annu. Rev. Biochem. *62*, 543–585.

Xie, Z., and Hendrix, R.W. (1995). Assembly in vitro of bacteriophage HK97 proheads. J. Mol. Biol. *253*, 74–85.

Yeager, M., Wilson-Kubalek, E.M., Weiner, S.G., Brown, P.O., and Rein, A. (1998). Supramolecular organization of immature and mature murine leukemia virus revealed by electron cryo-microscopy: implications for retroviral assembly mechanisms. Proc. Natl. Acad. Sci. USA *95*, 7299–7304.

Zlotnick, A., Cheng, N., Conway, J.F., Booy, F.P., Steven, A.C., Stahl, S.J., and Wingfield, P.T. (1996). Dimorphism of hepatitis B virus capsids is strongly influenced by the C-terminus of the capsid protein. Biochemistry *35*, 7412–7421.